

SUPPORTING INFORMATION

Catalytic applications of a versatile magnetically separable Fe-Mo(Nanocat-Fe-Mo) nanocatalyst

Manoj B. Gawande,^{*a} Paula S. Branco,^{*a} Isabel D. Nogueira,^b Amajd A. Ghumman,^c Nenad Bundaleski,^c
Adérito Santos,^c Orlando M.N.D. Teodoro,^c Rafael Luque,^d

^aREQUIMTE, Department of Chemistry, Faculty of Science and Technology, New University of Lisbon, Quinta da Torre,
2829-516 Caparica, Lisbon, Portugal

Email- m.gawande@fct.unl.pt; paula.branco@fct.unl.pt

Tel - +351-964223243, Fax: +351 21 2948550, Tel: +351 21 2948300

^bInstituto de Ciência e Engenharia de Materiais e Superfícies, IST, Lisbon, Portugal

^cCentre for Physics and Technological Research (CeFITec), Departamento de Física da Faculdade de Ciências
Tecnologia (FCT), Universidade Nova de Lisboa, 2829-516 Caparica, Portugal

^dDepartamento de Química Orgánica, Universidad de Córdoba, Edif. Marie Curie, Ctra Nnal IVa, Km 396, 14014
Córdoba, Spain

General methods and experimental	2
Optimization of reaction conditions.....	3
Spectral interpretation of synthesized compounds.....	4
TEM of Nanocat-Fe-Mo nanocatalyst.....	14
FEG-SEM of Nanocat-Fe-Mo.....	15
Histogram calculations	17
References.....	18

General methods and experimental

Experimental Techniques

All commercial reagents were used as received unless otherwise mentioned. For analytical and preparative thin-layer chromatography, Merck, 0.2 mm and 0.5 mm Kieselgel GF 254 percoated were used, respectively. The spots were visualized using UV light.

The X-ray powder diffraction pattern was obtained using a conventional powder diffractometer RIGAKU, model: MiniFlex™ II benchtop X-ray Diffractometer; X-ray tube: Cu-K α (30 kV / 15 mA) radiation operating in Bragg-Brentano ($\theta/2\theta$) geometry. (Sample preparation: grinding when needed and compression in the sample holder with a flat glass. The sample area in the sample holder is about 2 cm²). Transmission electron microscopy (TEM) experiments were performed on a Hitachi H8100 microscope, with a ThermoNoran light elements EDS detector and a CCD camera for image acquisition. The Fe₃O₄-MoO₃ fine powder was placed on carbon stub and the images were recorded at 5-15 kV using LFD detector under low vacuum.

Elemental analysis was done by using ICP-AES (Inductively coupled plasma-atomic emission spectrometer) using a Horiba Jobin-Yvon, France, Ultima, model equipped with a 40.68 MHz RF generator, Czerny-Turner monochromator with 1.00 m (sequential), autosampler AS500 and CMA (concomitant metals analyzer).

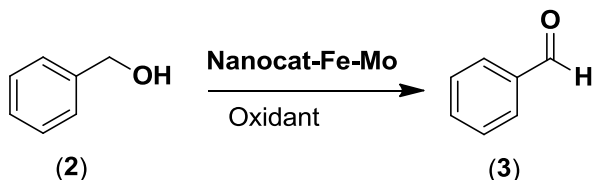
Scanning electron microscopy images were acquired using a JEOL JSM7001F FEG-SEM. Elemental analysis was performed using a light elements EDS detector from Oxford. The Fe₃O₄-MoO₃ powder was spread on a double-sided carbon tape and analyzed using 25kV acceleration voltage.

For SIMS, (secondary ion mass spectrometry) positive and negative secondary ion spectra were collected in the mass range of 0 -100 m/z (T=10 min) with an upgraded VG Ionex IX23LS TOF-SIMS set-up based on the Poschenrieder design. A focused liquid Ga⁺ gun in pulsed mode (6 kHz) was used as a source of the analytical ions. A beam current in dc mode at 14 keV was ca. 15 nA with a raster size of 300 X 300 μ m². Sample potential was 5 kV. Vacuum during the experiments was maintained in the range of (2-3) X10⁻⁹ mbar in the analytical chamber.

XPS measurements were performed on VSW XPS system with the Class 100 energy analyzer being a part of an experimental setup assembled for surface investigation. The spectra were taken in fixed analyzer transmission mode with the pass energy of 22 eV i.e. FAT 22. Fe₃O₄-MoO₃ fine powder was prepared for XPS by pressing on In (Indium) plate as a matrix in order to

reduce the charging problems and providing mechanical support. For the energy axis calibration Ag(110) and polycrystalline Au samples (previously cleaned by ion sputtering) were used. Proton NMR spectra were recorded on a Bruker, 400, 5 mm probe at 400 MHz. ^1H shifts are reported relative to internal TMS.

Table 1. Optimization of reaction conditions^a



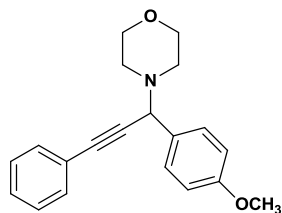
No.	Catalyst	Oxidant	Isolated Yield (%)
1	-----	-----	NR
2	-----	TBHP	NR
3	$\text{Fe}_3\text{O}_4\text{-MoO}_3$	-----	NR
4	$\text{Fe}_3\text{O}_4\text{-MoO}_3$	H_2O_2 (37 %) excess	NR
5	$\text{Fe}_3\text{O}_4\text{-MoO}_3\text{-50mg}$	TBHP	58
6	$\text{Fe}_3\text{O}_4\text{-MoO}_3\text{-100mg}$	TBHP	89
7	Fe_3O_4	TBHP	Trace
8	$\text{Fe}_3\text{O}_4\text{-MoO}_3\text{-100mg}$	TBHP (70 %)	65

Reactions condition : benzyl alcohol = 1mmol, TBHP 5-6 M in decane = 1 mL, catalyst = 100 mg (0.35 wt %), Temp = 80 °C, Time = 6 h.

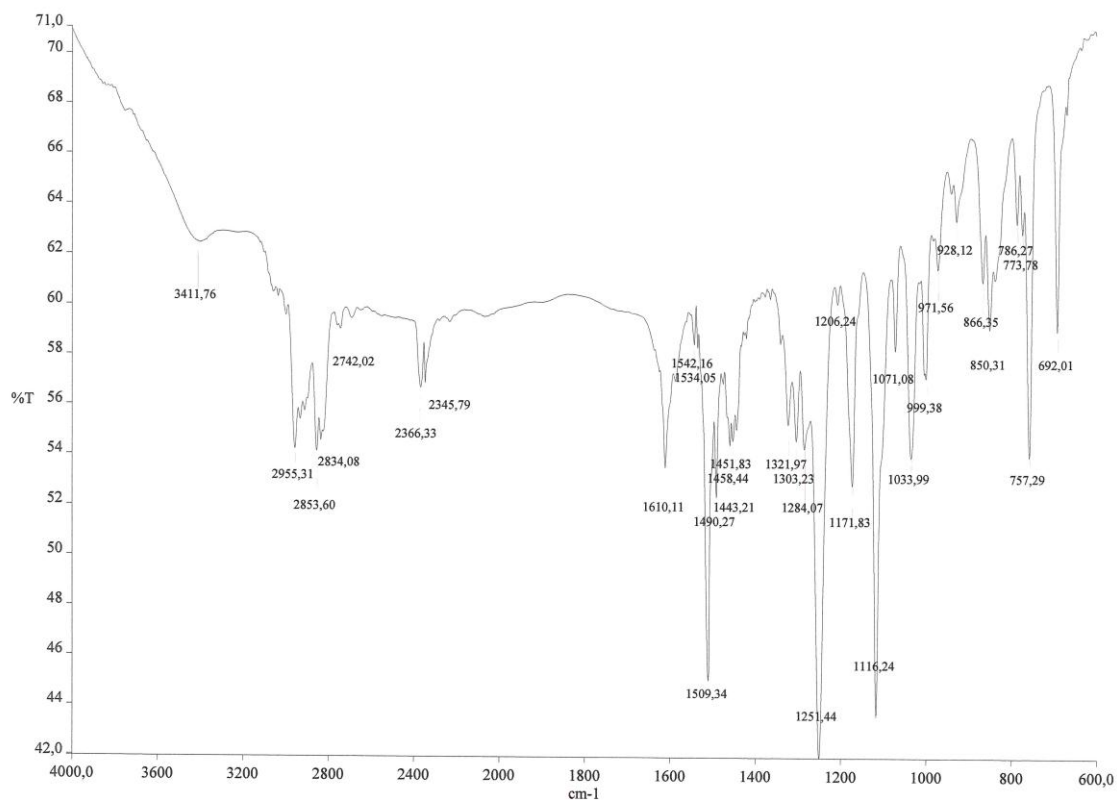
The oxidation of benzyl alcohol (2) to benzaldehyde (3) was used as a model reaction and the results are depicted in Table 1. Under catalyst-free and oxidant-free conditions no reaction was observed (Table 1 entries 1-3). Using H_2O_2 (37 %) as the oxidant the reaction did not succeed (Table 1, entry 4).

Using TBHP as the oxidant an excellent yield of 2 was obtained (89 %) in short reaction time (Table 1, entry 6). The Fe_3O_4 nanoparticle (30-35 nm, figure 1, a) gave only a trace amount of 2 (Table 1, entry 7). The yield of the reaction substantial increased when 100 mg of catalyst were used instead of 50 mg.

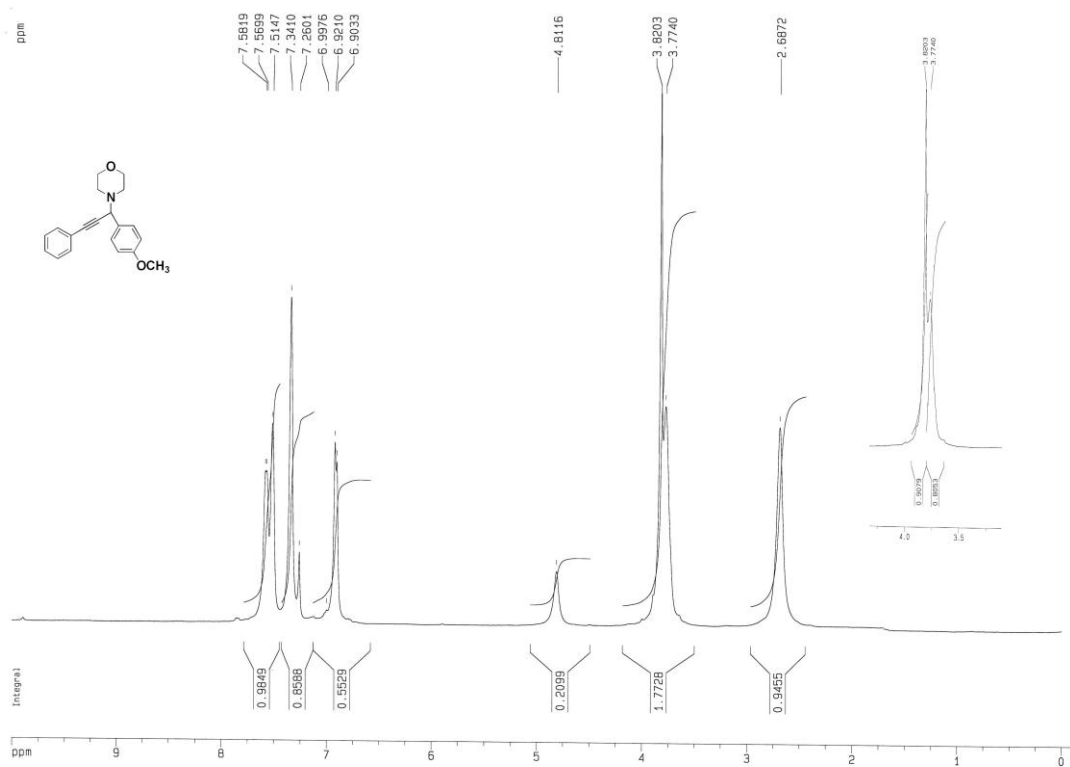
Spectral Interpretation of synthesized compounds



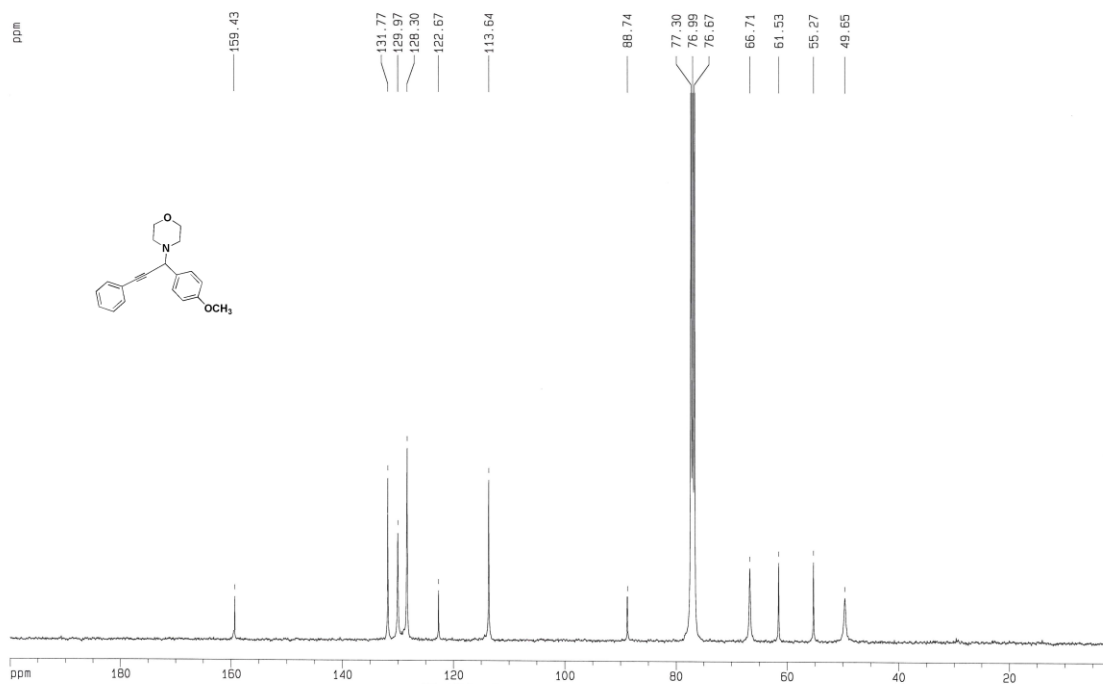
4-(1-(4-methoxyphenyl)-3-phenylprop-2-yn-1-yl)morpholine Obtained in 90 % yield; IR(KBr) ν_{max} : 1116, 1251, 1509, 2955; ^1H NMR (CDCl_3) δ : 7.58-7.51 (m, 4H), 7.34 (s, 3H), 6.91 (d, $J=8$ Hz, 2H), 4.81(s, 1H, -CH), 3.82(s, 3H, - OCH_3), 3.77 (bs, 4H), 2.68 (s, 4H); ^{13}C NMR, (CDCl_3) δ : 49.6, 55.2, 61.5, 66.7, 88.7, 113.6, 122.6, 128.3, 129.9, 131.7, 159.4. MSEI(+) m/z : 307.1, 219.6, 177.0, 94.5; HRMSEI(+) calcd for $\text{C}_{20}\text{H}_{21}\text{NO}_2[\text{M}]^+$ 307.1572 found 307.1573.



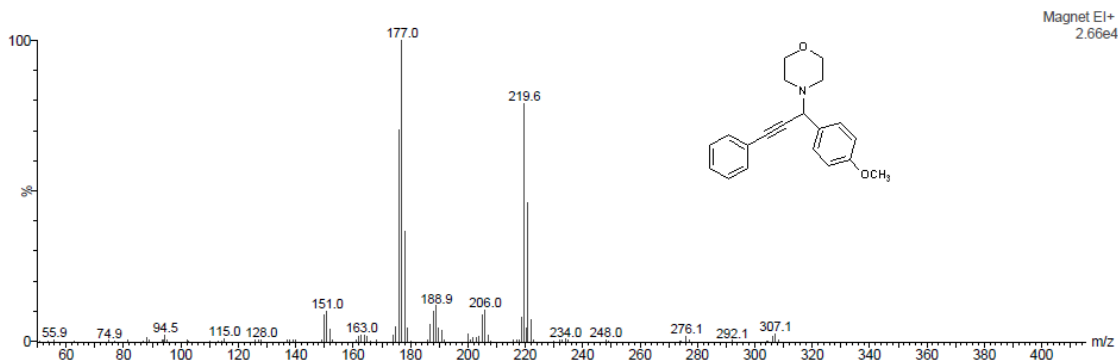
IR spectra of 4-(1-(4-methoxyphenyl)-3-phenylprop-2-yn-1-yl)morpholine (**9a**).



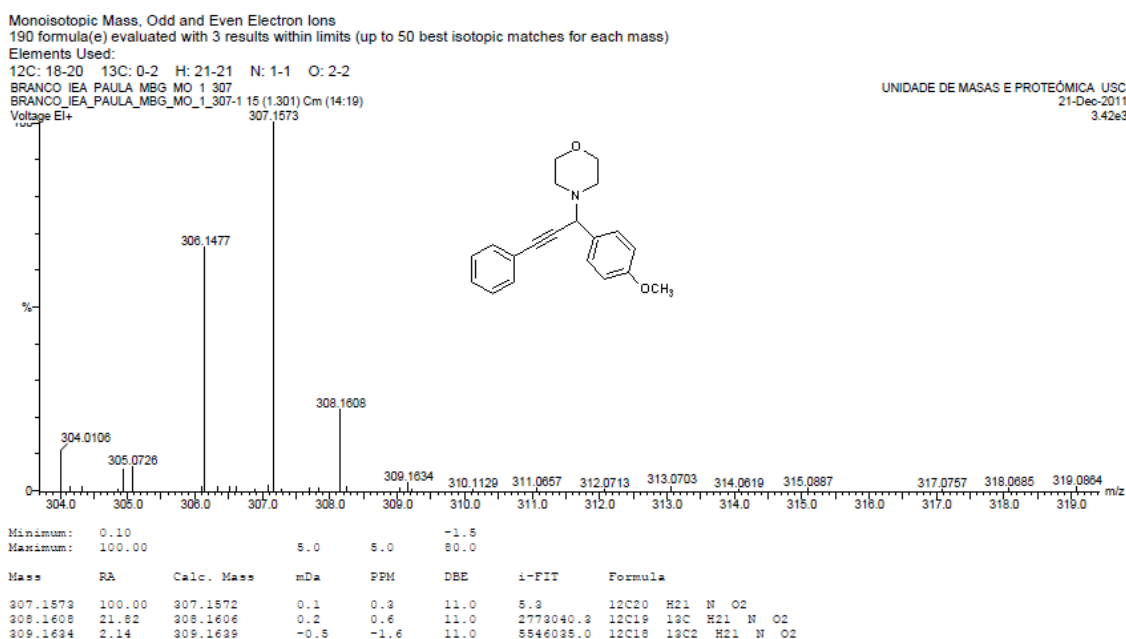
Proton NMR spectra of 4-(1-(4-methoxyphenyl)-3-phenylprop-2-yn-1-yl)morpholine (**9a**).



Carbon NMR spectra of 4-(1-(4-methoxyphenyl)-3-phenylprop-2-yn-1-yl)morpholine (**9a**).

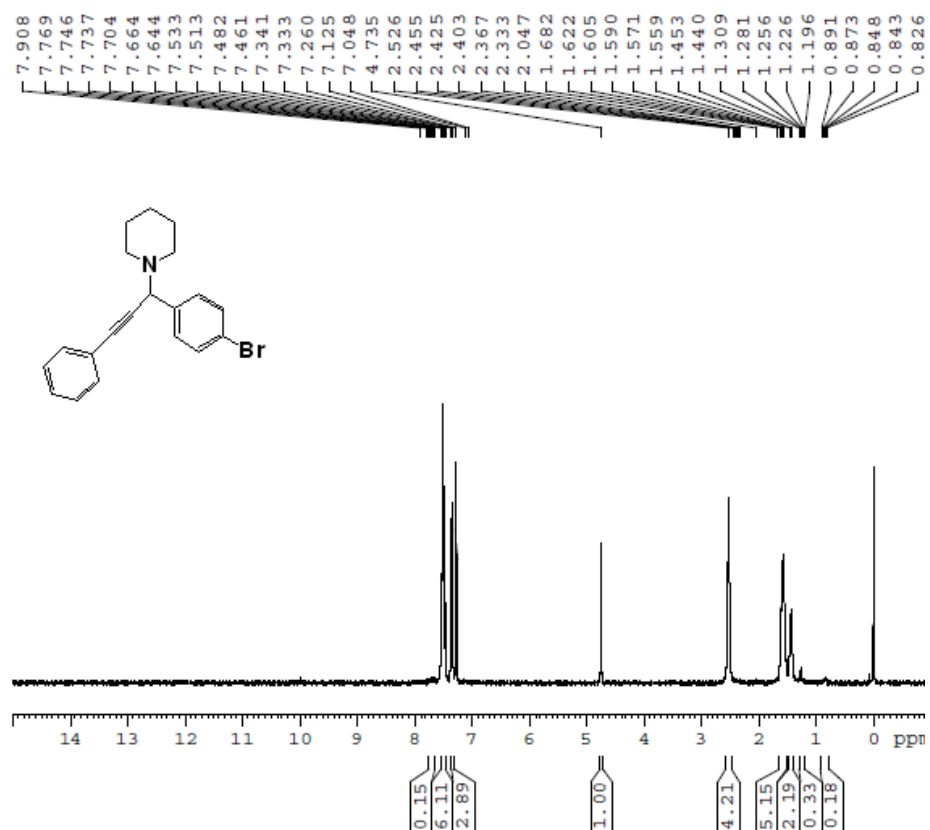


Electron impact mass spectra of 4-(1-(4-methoxyphenyl)-3-phenylprop-2-yn-1-yl)morpholine (**9a**).

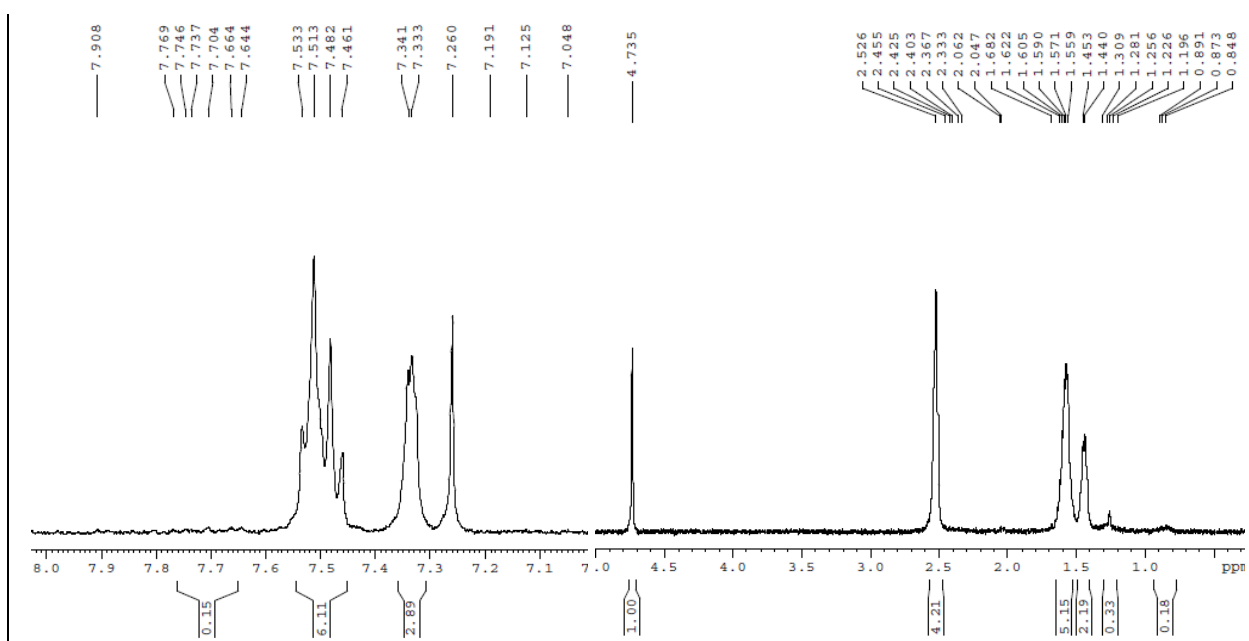


High resolution electron impact mass spectra of 4-(1-(4-methoxyphenyl)-3-phenylprop-2-yn-1-yl)morpholine (**9a**).

1-(1-(4-bromophenyl)-3-phenylprop-2-yn-1-yl)piperidine¹ (**9b**) obtained in 91 % ; ¹H NMR (CDCl₃) δ: 7.53-7.46 (m, 6H), 7.34-7.33 (m, 3H,), 4.73(s, 1H, -CH), 2.52 (m, 4H), 1.68-1.56 (m, 4H), 1.45-1.44 (m, 2H).

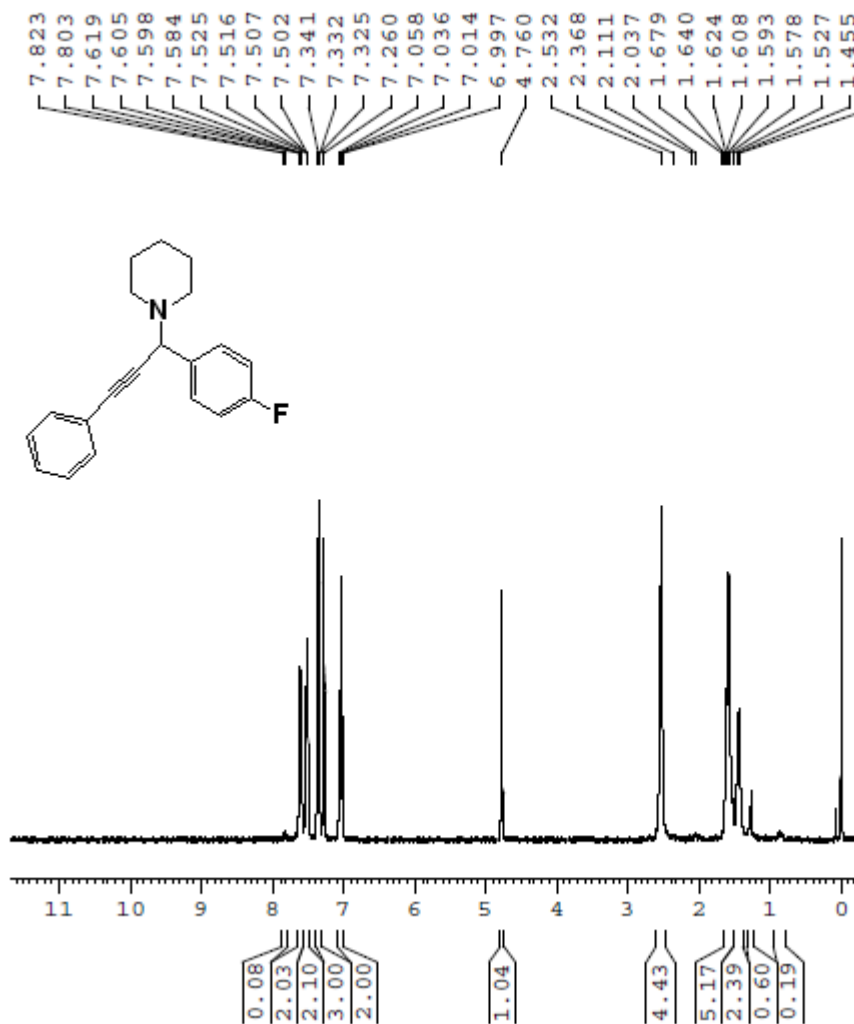


Proton NMR of 1-(1-(4-bromophenyl)-3-phenylprop-2-yn-1-yl)piperidine (**9b**)

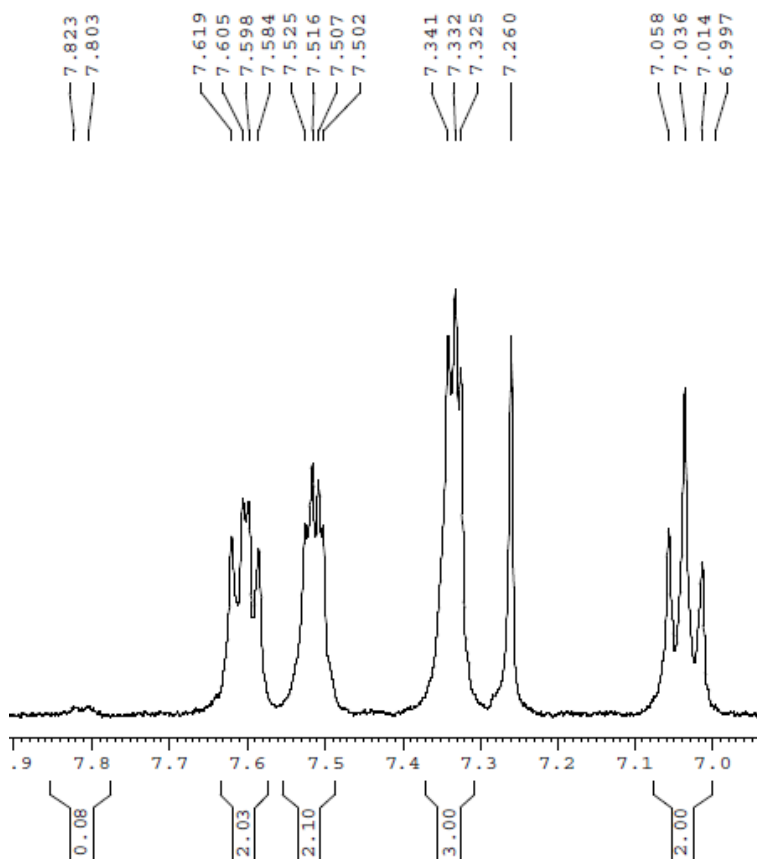


Expansion Proton NMR of 1-(1-(4-bromophenyl)-3-phenylprop-2-yn-1-yl)piperidine (**9b**)

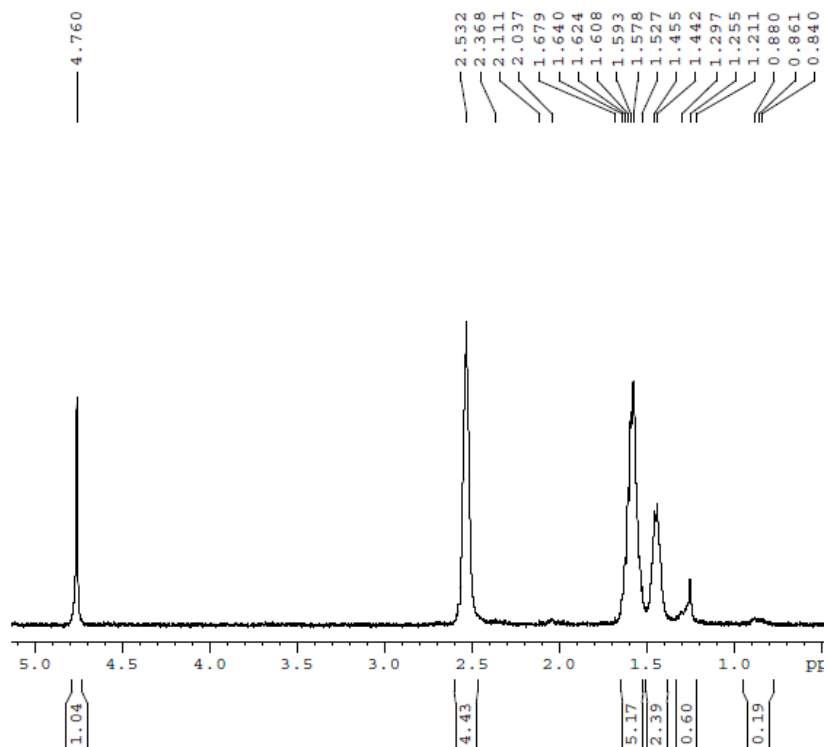
1-(1-(4-fluorophenyl)-3-phenylprop-2-yn-1-yl)piperidine² (**9c**) obtained in 90 %; ¹H NMR (CDCl₃) δ: 7.61-7.58 (dd, *J* = 8.4 and 5.6 Hz, 2H), 7.52-7.50 (m, 2H), 7.34-7.32 (m, 3H), 7.05 (t, 2H, *J* = 8.8 Hz), 4.76 (s, -CH), 2.53 (m, 4H), 1.67-1.45 (m, 6H).



Proton NMR of 1-(1-(4-fluorophenyl)-3-phenylprop-2-yn-1-yl)piperidine (**9c**)

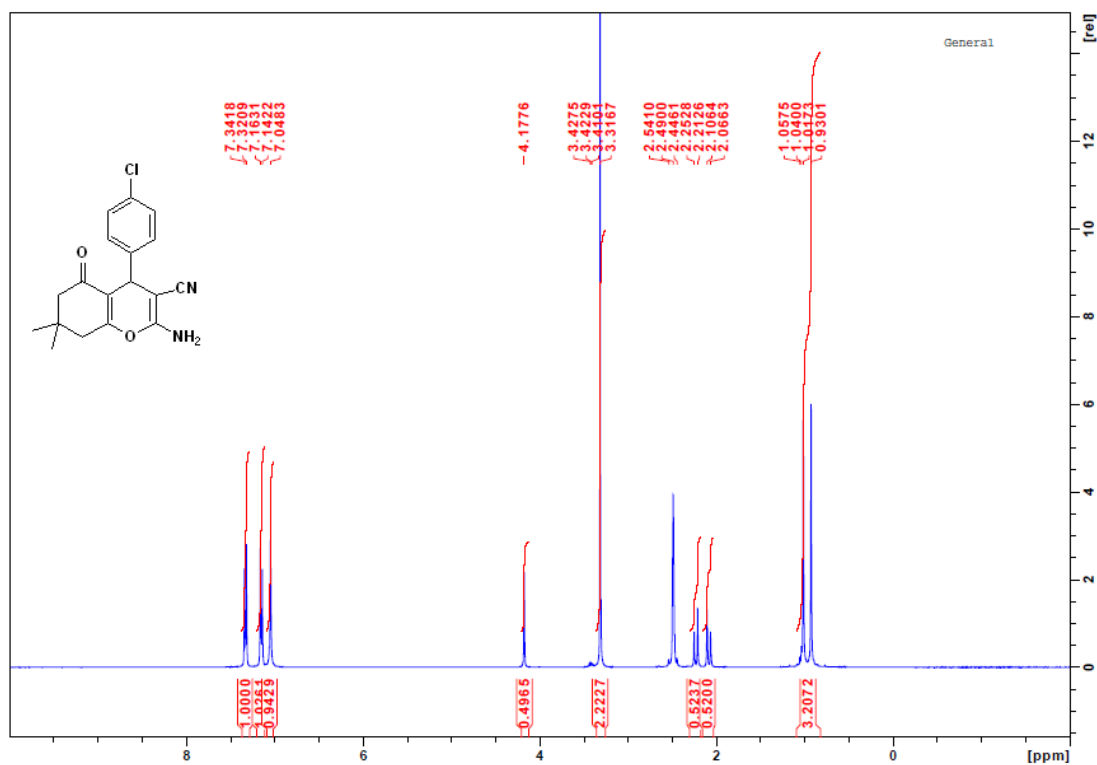


Expansion Proton NMR of 1-(1-(4-fluorophenyl)-3-phenylprop-2-yn-1-yl)piperidine (**9c**)

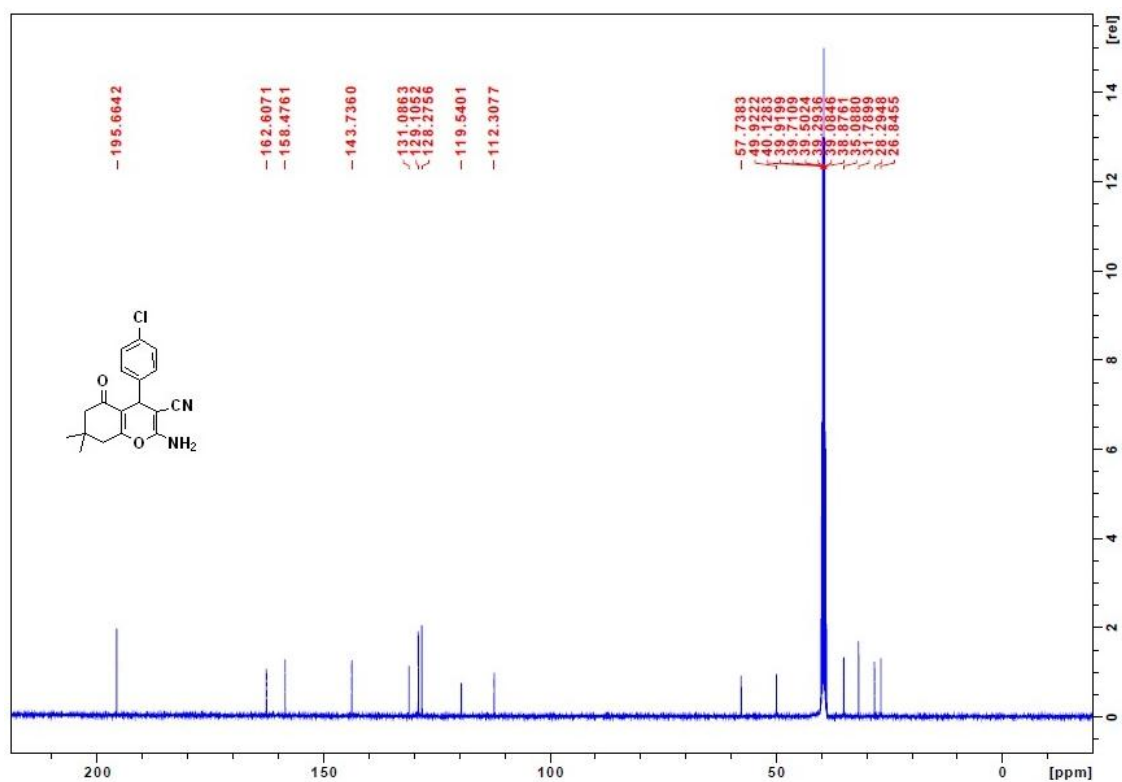


Expansion Proton NMR of 1-(1-(4-fluorophenyl)-3-phenylprop-2-yn-1-yl)piperidine (**9c**)

2-amino-4-(4-chlorophenyl)-7,7-dimethyl-5-oxo-5,6,7,8-tetrahydro-4H-chromene-3-carbonitrile³ (**15a**) obtained in 96 % yield ; ¹H NMR (400 MHz, DMSO) δ : 7.33 (d, $J = 8.4$, 2 H), 7.15 (d, $J = 8.4$, 2 H), 7.04 (bs, s, 2H, -NH₂), 4.17 (s, 1 H), 3.41 (bs, s, 2H), 2.23 (d, $J = 16$ Hz, 1H), 2.080 (d, $J = 16$ Hz, 1H), 1.01 (s, 3H), 0.93 (s, 3H); ¹³C NMR (DMSO) δ : 195.6, 162.6, 158.4, 143.7, 131.0, 129.1, 128.2, 119.5, 112.3, 57.7, 49.9, 35.0, 31.7, 28.2, 26.8.

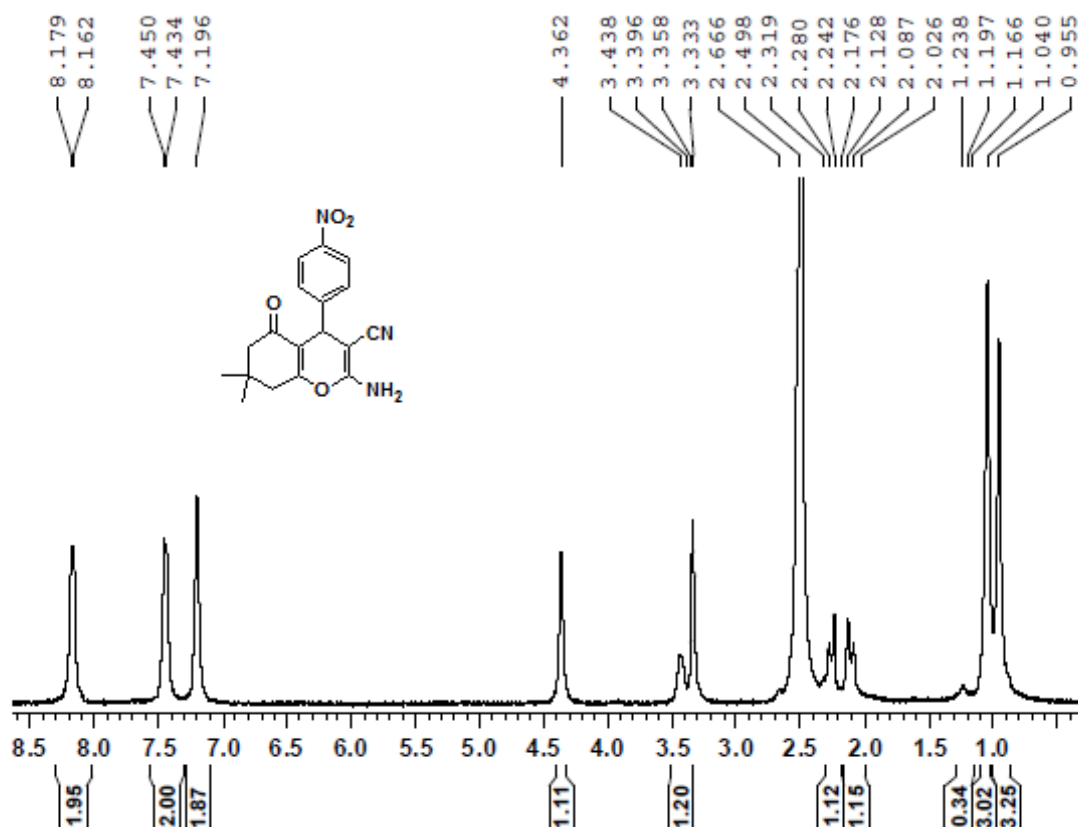


Proton NMR spectra of 2-amino-4-(4-chlorophenyl)-7,7-dimethyl-5-oxo-5,6,7,8-tetrahydro-4H-chromene-3-carbonitrile (**15 a**)



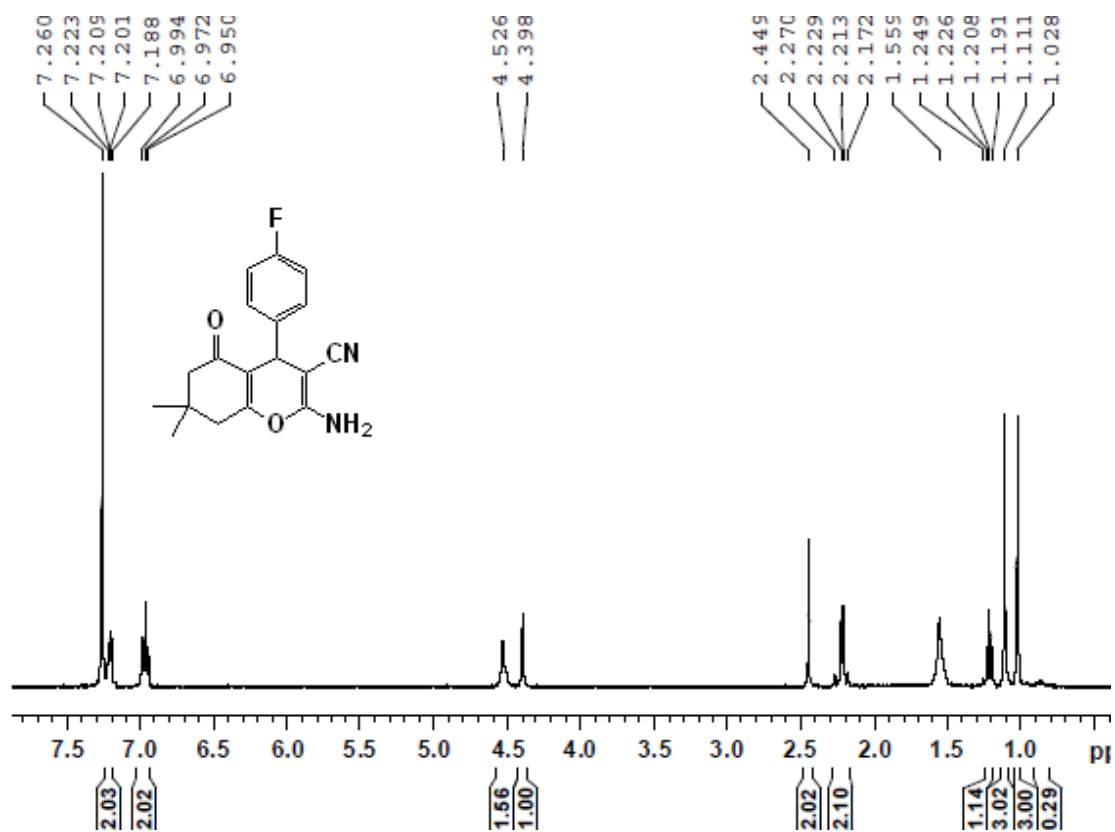
Carbon NMR spectra of 2-amino-4-(4-chlorophenyl)-7,7-dimethyl-5-oxo-5,6,7,8-tetrahydro-4H-chromene-3-carbonitrile (**15a**)

2-amino-7,7-dimethyl-4-(4-nitrophenyl)-5-oxo-5,6,7,8-tetrahydro-4H-chromene-3-carbonitrile⁴ (**15b**) obtained in 90 %; ¹H NMR (400 MHz, DMSO) δ : 8.17 (d, J = 6.8 Hz, 2 H), 7.45 (d, J = 6.4 Hz, 2 H), 7.19 (bs, s, 2H, -NH₂), 4.36 (s, 1 H), 2,5 (bs, 2H, under the peak of DMSO), 2.31-2.24 (m, 2 H), 2.17-2.02 (m, 2 H), 1.04 (s, 3H), 0.95 (s, 3H).



Proton NMR of 2-amino-7,7-dimethyl-4-(4-nitrophenyl)-5-oxo-5,6,7,8-tetrahydro-4H-chromene-3-carbonitrile (**15b**)

2-amino-4-(4-fluorophenyl)-7,7-dimethyl-5-oxo-5,6,7,8-tetrahydro-4H-chromene-3-carbonitrile³ (**15 c**) obtained in 92 %; ¹H NMR (400 MHz, CDCl₃) δ : 7.20 (dd, *J* = 8.6 and 5.4 Hz, 2 H), 6.97 (t, *J* = 8.8 Hz, 2 H), 4.52 (bs, s, 2H, -NH₂), 4.39 (s, 1 H), 2.25 (d, *J* = 16.4 Hz, 1 H), 2.19 (d, *J* = 16.4 Hz, 1H), 1.24 (d, *J* = 8 Hz, 1H), 1.20 d, *J* = 8 Hz, 1H), 1.11 (s, 3H), 1.02 (s, 3H).



Proton NMR of 2-amino-4-(4-fluorophenyl)-7,7-dimethyl-5-oxo-5,6,7,8-tetrahydro-4H-chromene-3-carbonitrile (**15 c**)

Transmission electron microscopy (TEM)

Transmission electron microscopy (TEM) experiments were performed on a Hitachi H8100 microscope, with a ThermoNoran light elements EDS detector and a CCD camera for image acquisition. The TEM of ferrite and Nanocat-FeMo MNPs shows uniform-sized magnetic nanoparticles and showing somewhat spherical morphology with an average size range of 15–30 nm (Figure 1).

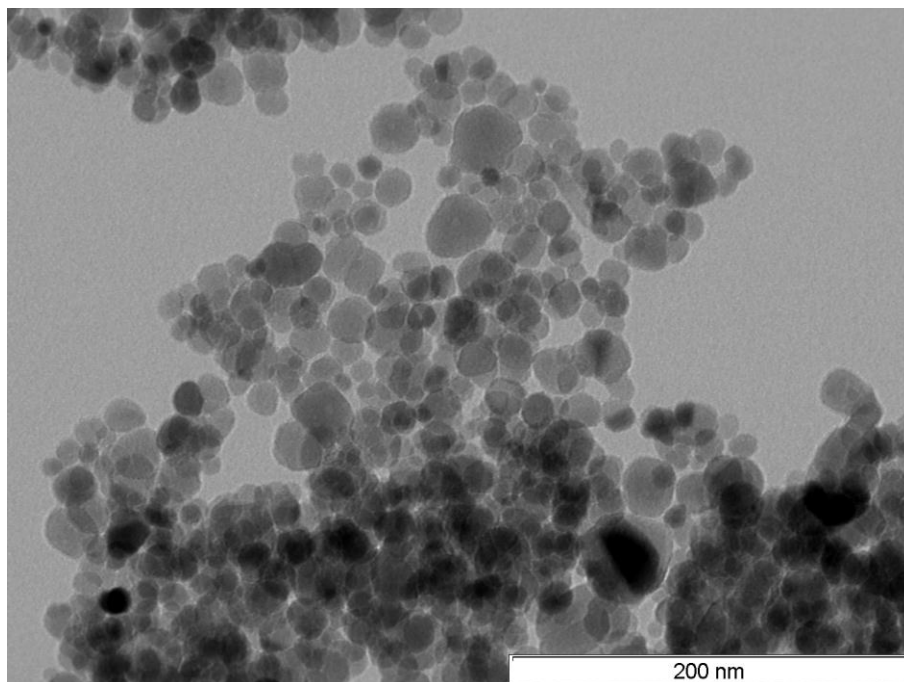


Figure 1 a) TEM image of Ferrite at 200 nm

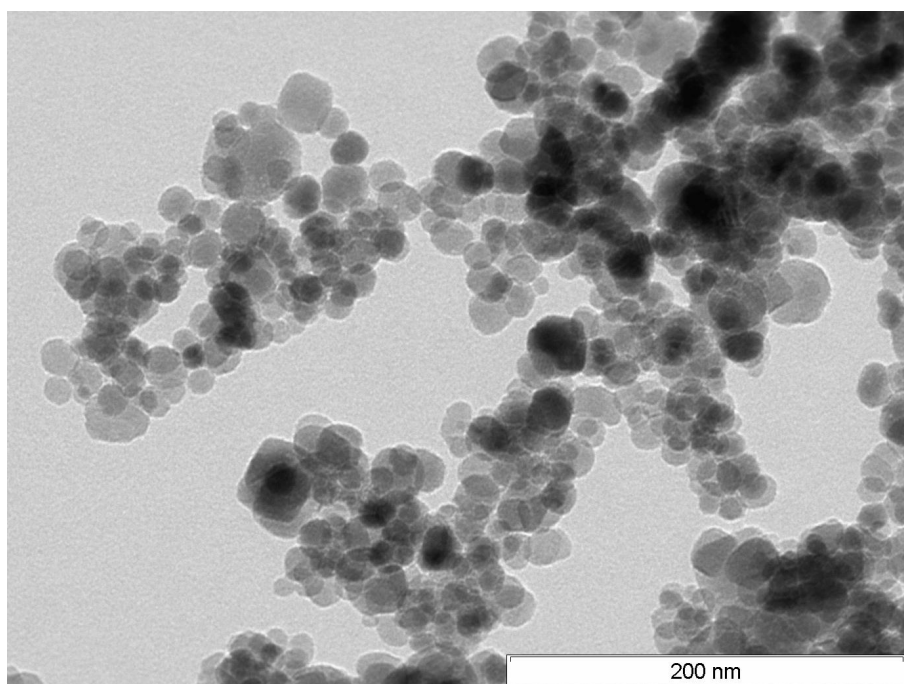
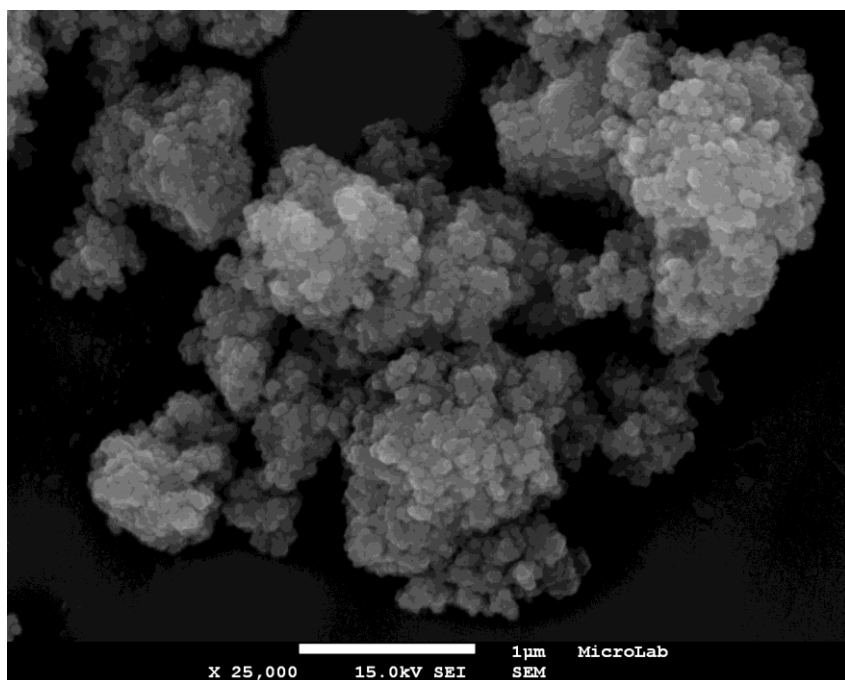


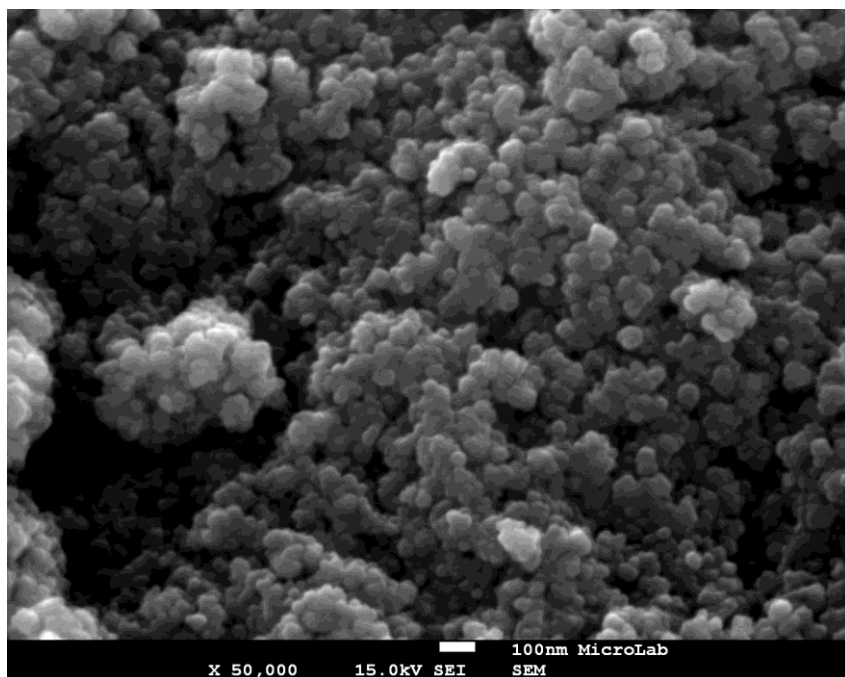
Figure 1b. TEM image of Nanocat-Fe-Mo nanoparticles

FEG-SEM of Nanocat-Fe-Mo

For analysis on the FEG-SEM the sample was observed using 25kV acceleration voltage. The images show uniformly-size particles, with somewhat spherical morphology of the particles and look like wooly cloud like clusters (Figure 2).



2a)



2 b) Figure 2. SEM images of Nanocat-Fe-Mo nanoparticles

Histogram Calculations

In order to build the histogram for the particle size distribution of Nanocat-Fe-Mo, a large number of images (10 to 15) were acquired from each sample (for example two representative image are shown below Figure 3 b) and the size of the particles on the border area was measured.

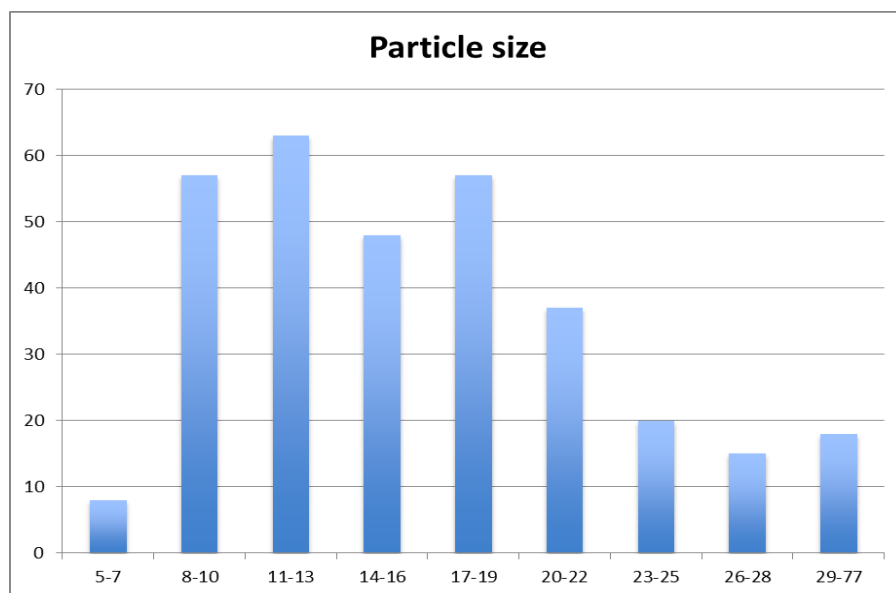


Figure 3a) Histogram showing particle size distribution of Nanocat-Fe-Mo

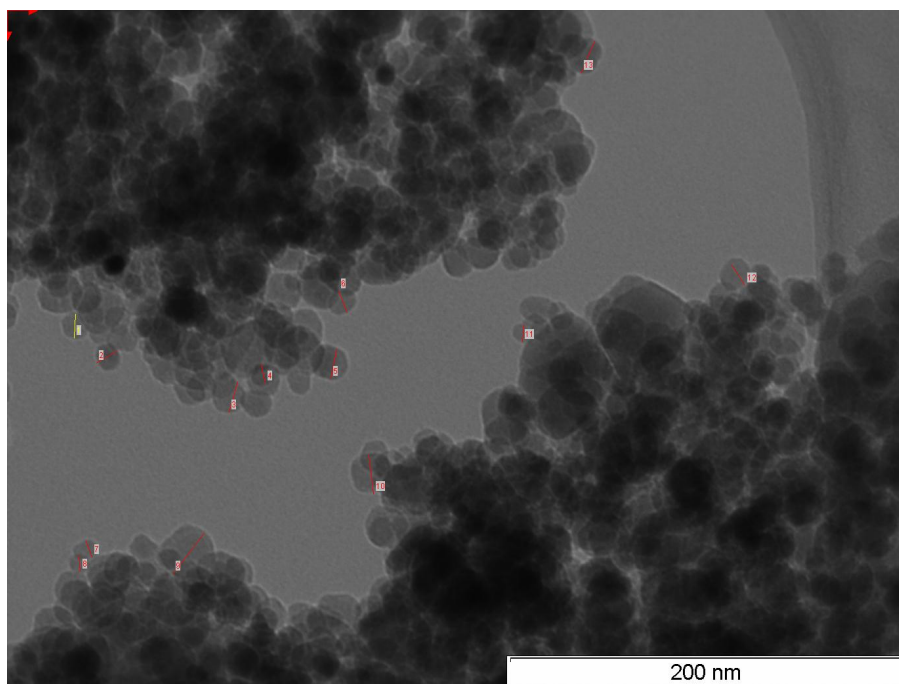


Figure 3 b) Representative TEM image of Nanocat-Fe-Mo for histogram calculation.

References

1. K.V.V. Satyanarayana, P. A. Ramaiah, Y.L.N. Murty, M. R. Chandra, S.V.N. Pammi, *Catal. Commun.* 2012, 25, 50–53.
2. S. Samai, G. C. Nandi, M. S. Singh, *Tetrahedron Lett.* 2010, 51, 5555–5558
3. L. Rong, X. Li, H. Wang, D. Shi, S. Tu, Q. Zhuang, *Synth. Commun.* 2006, 36, 2363–2369.
4. J. Marco-Contelles, R. Leo'n, C. de los Rios, A. G. Garcia, M. G. Lopez, M. Villarroya, *Bioorg. Med. Chem.* 2006, 14, 8176–8185